Calculating structural and electronic properties of MXene Ta_2C with surface terminal groups

Adam L. Smith

Department of Physics, University of Bath, Bath BA2 7AY, United Kingdom
Email: as3359@bath.ac.uk
Thursday 5th May, 2022

Abstract. The development of new electronic devices is dependent on the discovery of new materials with particular electronic properties. Computational material modelling with density functional theory (DFT) has enabled the scientific community to understand how MXenes, $M_{n+1}X_n$, can be implemented in new technology. Investigations into the influence a surgace terminal group can have on an MXene such as Ta_2C is yet to be investigated. By using the open source Quantum ESPRESSO package, the crystal and band structure were determined. Furthermore, it was confirmed that Ta_2CT_x is a metal for the terminal groups T_x = [H_2, O, O_2, S]. Thus, these materials would be suitable conductive materials.

1. Introduction

The 2D transition metal carbide and nitride materials called MXenes have been at the forefront of research in material science in the past decade [1]. They have a wide range of applications which extends to supercapacitors, sensors and biomedical materials [2]. Across many industries, there is a demand for newly developed materials that consist of more ideal mechanical, structural and/or electrical properties. For example, the UK government has pledged that the production of all new petrol and gas fuelled cars will be banned, empathising the need for more electric cars on UK roads by 2030. A challenge for the emergence of better performing lithium batteries has been due to the lack of effective electrode materials used to to improve the ionic flow of charge across the electrodes from the battery itself [3]. These materials also have applications for the biomedical industry [4].

MXenes are generally formulated by $M_{n+1}X_n$, n $\geq$ 1, where M denotes the early transition metal that is interleaved with n layers of carbon or nitrogen, denoted X. MXenes are commonly synthesized in practice by the chemical etching of structures called MAX phases, $M_{n+1}AX_n$, where A is an A group element such as Aluminium [5]. Chemical etching is a process that is used in order to isolate MXene structures from the MAX phases. By etching out the A layers, typically an element from the group 13-16, the MXene nanosheets desired can be created [6]. MXenes in their general structure tend to be a metal. In the case where the number of electrons in the unit cell is odd, there is at least a band that is partially occupied. This contributes to the

conductive properties of a material. Therefore, the material is a metal. Each band can occupy up to 2 electronic states in line with the Pauli Exclusion Principle [7]. A semiconducting material such as molybdenum disulphide, MoS_2, can be designed as a direct semiconductor by reducing the material to a monolayer structure [8]. Otherwise, in bulk it is an indirect semiconducting material. Another approach to influence a change in the electrical properties, can be to introduce surface terminal groups, T_x, to form $M_{n+1}X_nT_x$ [9]. Being able to discover new potential applications to such materials could be vital for the development for in demand technology.

In order to progress how quickly material discovery can happen, it is possible to use computational techniques to describe and predict the properties of a material quantitatively. In 1925, Schrödinger formulated a method to model the probability density of a particle in real space using a system governed by a linear partial differential equation. The basic elements of Quantum Mechanics can be used extensively in molecular modelling and furthered to a many body problem, ref [10]. After Dirac was able to model the simplest of atoms in the periodic table using the Schrödinger equation, the Hartree-Fock theory developed an algorithm that could model a many body quantum mechanical system by the means of variational principle to establish the ground state energy of a system [11]. As a consequence, the Kohn-Sham Density Functional Theory (DFT) was published 40 years after the original publication from Schrödinger [12]. The development of these techniques have enabled these calculations to not be restricted to calculations over a single atom, diatomic or highly symmetrical structures. With the introduction of high performance computers (HPC) in the mid 1980's, these calculations can be done without the need of long hand computation. In addition, this can prove to save on resources developing these materials in a laboratory. Thus, in this project a HPC is fundamental to the computational experimentation that will be on show. A package such as Quantum ESPRESSO (QE) can be used to calculate the crystal and band structure of these materials. In QE, there are two types of structural optimization calculations. The relax calculation allows only the atomic positions to vary in order to optimize the structure. Whereas a variable cell relax (VC-Relax) varies both the atomic positions and the lattice vectors. The self-consistent field (SCF) calculation is an iterative method that involves selecting an appropriate Hamilitonian to solve the Schrödinger equation to obtain a more accurate set of orbitals until these results converge. A non-self-consistent field calculation is explicitly the calculation in the SCF but without checking for self consistency. As a consequence to these calculations, the band structure and density of states can also be calculated using QE. The MXene in this project that was modelled using these methods was Ta_2C. Many of the early transition metals such as Ti, Sc and Zr have been investigated over the past few years [5]. Ta_2C has interest for its excellent conductivity levels. Ta_2C is known for being an excellent electrode material. Notably, the characteristics of a material have been altered due to the introduction of surface terminal groups (e.g F, Cl, O_2) [9, 13]. In particular, the surface terminal groups F, O and O_2 are likely results of the aqueous hydrofluoric acid etching.

Here we show how DFT using the Quantum ESPRESSO package, is used to calculate the total energy, the band structure and the density of states (DOS) for Ta_2C crystal structure [14, 15, 16]. This has been achieved through a variable cell relaxation (VCR), relaxation, (non-)self consistent field (NSCF/SCF), bands and DOS calculations. The electronic properties of Ta_2C will be investigated to confirm it is a metal. The influence of surface terminal groups on these calculations will also be demonstrated to determine if these structural changes influence the electronic behaviour of the MXene.

2. Theory

DFT is one of the most popular computational modelling techniques used for solid state calculations. For real materials, in order to understand their physical properties, a calculation of the electronic structure by an *ab-initio* method (quantum chemistry method) is used [17]. Quantum particles are described by the wavefunction. For the case of an electron in a potential field, V, its wavefunction is calculated by solving the Schrödinger equation

$$-\frac{\hbar^2}{2m}\nabla^2\Psi(\mathbf{r},t) + V(\mathbf{r},t) = i\hbar\frac{\partial\Psi(\mathbf{r},t)}{\partial t}, \tag{1}$$

where $\hbar$ is the reduced Planck constant and Ψ the wavefunction solution. In order to describe any N-electron system we have to solve Schrödinger's equation $\mathcal{H}\Psi = \mathcal{E}\Psi$, where total energy, $\mathcal{E}$ of the system can be determined by a Hamiltonian operator, $\mathcal{H}$. In this project, the electrons that are being modelled are subject to the Coulomb interactions from the nucleus and the other electrons. As the nucleus is heavy, the motion of the electrons is much slower than conduction electrons that are free to move around the solid. Thus, it can be assumed for this model that the potential field is not a function of time, t. Therefore, the wavefunction can be made separable into its spatial and temporal components $\Psi(\mathbf{r},t) = \psi(\mathbf{r})f(t)$. Then, equation (1) reduces to the time independent Schrödinger equation

$$\Big(-\frac{\hbar^2\nabla^2}{2m} + v(\mathbf{r})\Big)\psi(\mathbf{r}) = \epsilon\psi(\mathbf{r}), \tag{2}$$

where ϵ denotes the total energy of the time independent system.

2.1. Hohenberg-Kohn Theorems (HKT)

By focusing on the electronic density instead of the wavefunctions themselves, DFT minimizes the energy of a system in a self consistent way (avoiding any contradiction throughout the calculations). The HKT states

I. Ground state density $n(\mathbf{r})$ determines the external potential energy to the material $v(\mathbf{r})$ to within a trivial additive constant

II. Total Energy of the system $\mathcal{E}(n)$ is minimal when $n(\mathbf{r})$ is the actual ground state density, among all possible electron densities [18].

What separates these theorems from the Schrödinger equation is that it is possible to define the ground state energy as a function of electronic density. This can be done by minimizing $\mathcal{E}(n)$ [18]. In reality, the exact $\mathcal{E}(n)$ will be unknown and thus, the calculations used in this project are only approximate. The total energy of an interacting inhomogeneous electron gas in the presence of an external potential $V_{ext}(r)$ is

$$\mathcal{E} = \int V_{ext}(\mathbf{r})n(\mathbf{r})d\mathbf{r} + \mathcal{F}[n], \tag{3}$$

where the potential is a functional of the density n and $\mathcal{F}(n)$ is an unknown functional of the electron density. This gives rise to $\mathcal{H} = T(n)+V_{eff}(n)$, the conservation of energy equation in terms of their respective linear operators.

2.2. Kohn-Sham Equations (KSE)

The KSE are central to the first principles of material modelling [12]. The KSE extend the HKT by introducing an extra energy correction. The electronic correlation correction is a measure of how the movement of one electron in a quantum system is influenced by the presence of all other electrons [19]. Thus, taking all of the assumptions from HKT and the KSE the single particle equation follows

$$\Big(-\frac{\nabla^2}{2} + V_n(\mathbf{r}) + V_H(\mathbf{r}) + V_{XC}(\mathbf{r})\Big)\phi_i(\mathbf{r}) = \epsilon_i\phi_i(\mathbf{r}) \tag{4}$$

where V_n is the coulomb potential, V_H the Hartree potential, V_{XC} the exchange correlation energy and i denoting each electron.

2.3. Algorithmic implementation of DFT

The solution ϕ_i to the KSE from equation (4), must depend implicitly on all other solutions, ϕ_j describing occupied states [17]. Given all of these solutions depend on each other, they must all be determined self consistently. The algorithmic approach in figure 1 shows how the solutions for the KSE were obtained. The wavefunction is estimated based on the atomic orbitals. Then by constructing the first guess for the electron density, the computation is able to make a very useful first approximation. Using the electron densities, the initial estimates of the Hartree and exchange-correlation potentials can be made. Thus, the process of finding the numerical solution of the KSE can begin. By solving the KSE and obtaining new wavefunctions, ϕ_i, a better estimate of the electron density and total potential is constructed. Then this process is repeated until the new density calculated by

$$n(\mathbf{r}) = \sum_i |\phi_i(\mathbf{r})|^2, \tag{5}$$

is within a desired tolerance from the previous density calculated. At this point, the self-consistency has been achieved. Once the electron density in the ground state has been obtained, the total energy $\mathcal{E}$ can be calculated and subsequently, it can be used to calculate other properties about the material.

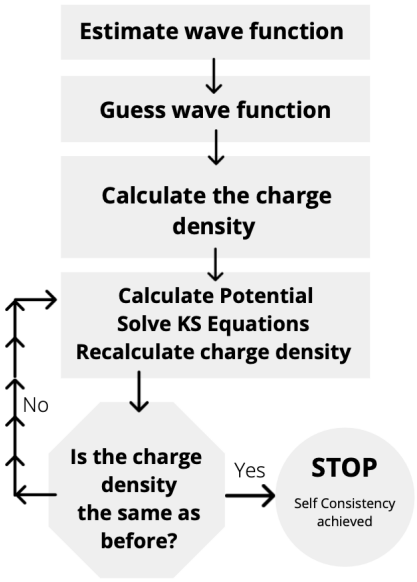

Figure 1: Schematic flow-chart demonstrating how the self-consistent solutions to the Kohn-Sham equations are found. The algorithm stops when the electron density at this particular iteration, and the density in the previous iteration, only differ by a desired tolerance.

2.4. Band calculation

In order to calculate the approximate energy eigenvalues and eigenstates of the material, calculating the band structures requires the use of Bloch Theorem [17]. The total energy of the system is calculated by

$$\mathcal{E} = \sum_i f_i \epsilon_i - [\mathcal{E}_H + \int d\mathbf{r} V_{xc}(\mathbf{r}) n(\mathbf{r}) - \mathcal{E}_{xc}], \tag{6}$$

where f_i, the Fermi Dirac distribution, $\mathcal{E}_{\mathcal{H}}$ is the Hartree energy term, V_{XC} is the exchange correlation term and $\mathcal{E}_{\mathcal{XC}}$ is the exchange correlation energy. The first term is the sum of the energies of all the occupied Kohn-Sham states, and is referred to as the band structure energy. The second term contains the necessary conditions to avoid any double counting of the same total energy contributions.

2.5. Pseudopotentials

For a model to be able to calculate over every Kohn-Sham state would be computationally expensive and time consuming as rapid variation of $V(\mathbf{r})$ near the core requires very large values of $\mathbf{k}$, therefore many plane waves would need to be considered. The number of plane waves can be reduced significantly by the use of a pseudopotential (PP) [20]. A PP is a modification of the ionic potential which allows the number of plane waves required to be reduced. Due to the lack of interactions that occur with the core electrons of a material, it is a reasonable approximation if these core electrons were frozen out of the calculation. Therefore, only the valence electrons will be considered.

This makes the plane wave basis sets for the electronic wavefunctions more practical to use. Without the use of pseudopotentials, the study of systems of many atoms similar to the ones explored here would not be possible.

3. Computational Methods

The theory discussed previously was implemented in an integrated suite of Open-Source computer codes called Quantum ESPRESSO (QE) [14, 15, 16]. All of the code and data plots are made publicly availible on github at: *https://github.com/adamlsmith981/SmithAdamFYP* . These calculations are developed from DFT, plane waves and pseudopotentials [17]. The method follows the sequential procedure of performing these calculations in order:

I. Variable cell relax (VCR) and relax loop

II. Convergence testing for:
    - energy cut off
    - number of k points
    - lattice constant

III. Identify the k path on the Brillouin zone

IV. Bands and density of states (DOS) calculations.

For demonstration purposes, a material that is well researched such as MoS_2 will be experimented on [8]. In this section, computational methods are presented to show how the figures and calculations were obtained.

3.1. Modelling assumptions

The ultrasoft pseudopotentials (PP) generated by the RRKJ method were used in these calculations. An ultrasoft method for producing the plane waves that model the valence electronic states relaxes the norm-conserving constraint in order to reduce the necessary basis set further [21]. A norm-conserving pseudopotential required that each pseudo wavefunction carries exactly one electron. PBEsol PP's were preferred over PBE functionals. This is because PBEsol considers the second order gradient expansion for the exchange energy, where PBE fails to. It also can account for the medium range interaction better than the PBE potentials. In addition, PBEsol is more refined for solid materials.

3.2. QE input parameters

The QE package has the freedom to choose various techniques or threshold parameters that are considered in the final calculations. The use of Conjugate-gradient-like (cg) band to band diagonalization was used at times in order to achieve convergence. This is much slower than the Davidson diagonalization method, but proves to be more robust when calculations get tricky. The use of smearing was also helpful to aid convergence. The Marzari-Vanderbilt-DeVita-Payne cold (m-v) smearing is adopted to aid the convergence of the calculations. The guassian spreading (deguass) used

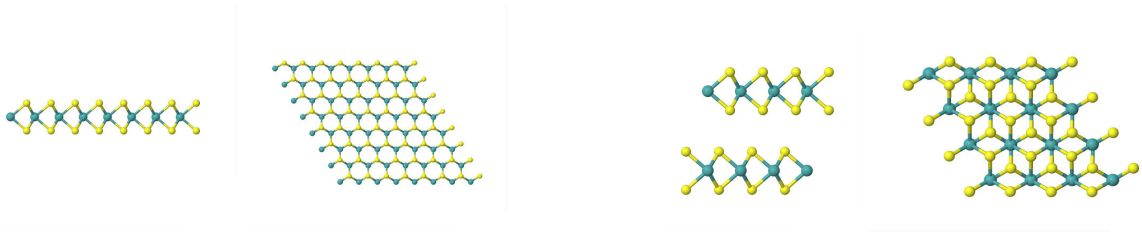

(a) (b)

Figure 2: Presenting the heterostructures of (a) monolayer and (b) bilayer MoS_2 using Jmol from a lateral and top down view. (a) Monolayer MoS_2 crystal structure with lattice constant 3.137 Å. (b) Bilayer MoS_2 crystal structure with lattice constant 3.140 Å. In (a) and (b) the bond length was 2.39 Å between Mo (blue) and S (yellow) atoms. In (b) the Layers are anti-parallel i.e 180° rotation in the xy plane and the layer separation was 6.52 Å between adjacent Mo atoms.

was 13.6 meV. This smearing technique introduces an electronic temperature. At zero temperature, the occupations drop abruptly to 0 as the corresponding energy eigenvalues become larger than the Fermi energy [22]. The calculations assume that the material is at absolute zero, a consideration required when analysing the density of states calculations. Instead, a natural choice would be to use the Fermi-dirac distributions. However one needs to use very large values in order to make the k point sampling better since the distribution itself has long tails and one would need to calculate a relatively large number of states [23].
All code was submitted to run on the University of Bath HPC, Janus. This was on partition *spot-fsv2-64*. All code can be accessed on the github provided.

3.3. VCR loop

In QE there are two given types of calculations for structure optimization: relax and vc-relax. These both allow for the variation of both atomic positions and lattice constants in order to obtain a stable structure. The latter is computationally more expensive as it looks to optimize the cell parameters with both the forces and stress tensor calculated. The relax calculations only optimize the atomic coordinates.
In figure 2, the optimised structures for MoS_2 are visualised from the output calculations of QE using Jmol: an open-source Java viewer for chemical structures in 3D. http://www.jmol.org/. In order to make sure the structures modelled were in isolation to repeating structures, a vacuum gap of ≈ 30 Bohr was implemented. In this project, the process of finding an optimised structure was automated. Through an iterative process, the VCR and relax calculations would be done sequentially, with the previous parameters being thread into the next calculation. The energy convergence threshold was set to 2.72 meV and the force convergence was set to 10^{-10} N. The pressure convergence threshold was set to 1.0 kbar. The script optimizes the structure until pressure and force convergence was achieved. For MoS_2 monolayer and bilayer, the

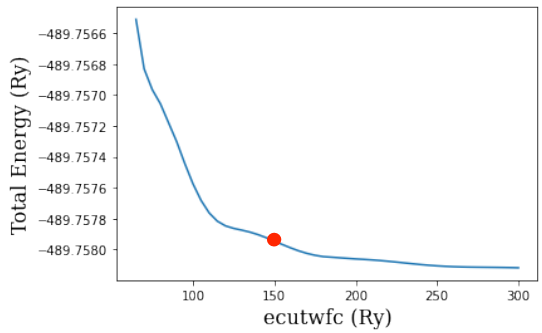

(a) ecutwfc convergence test. The rate of change drops significantly past 150 R_y.

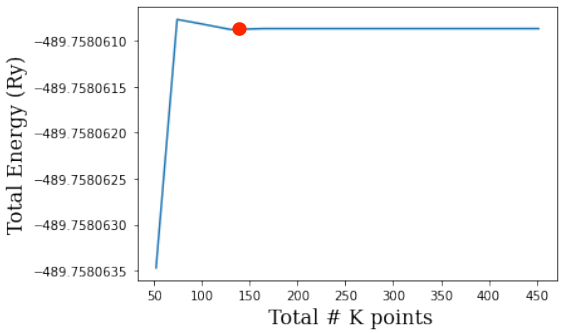

(b) K points convergence test. Convergence is achieved between 100 and 150 k points.

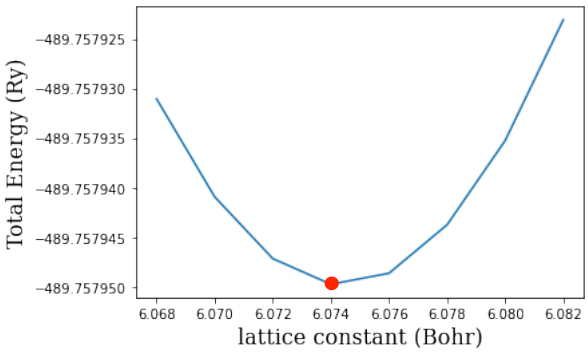

(c) Lattice parameter convergence test: 6.074 Bohr coincides with being the minimum point of the convergence test.

Figure 3: The convergence tests for monolayer MoS_2 across 3 parameters: kinetic energy cutoff, k points and the lattice constant. Convergence testing is an important part of producing the ultimate model in the final step where the bands and DOS calculations are made. For the final calculations of monolayer MoS_2, the ecutwfc was set to 150 R_y, a 15 by 15 by 1 k point grid and a lattice constant of 6.074 Bohr.

optimized structures were able to achieve a computational pressure of -0.45 kbar and -0.85 kbar respectively. Values that are close to 0 kbar invoke a stable structure at 0 K. in 2016, the lattice constant for monolayer MoS_2 was determined to be 3.17 Å[24]. This is within 1% of the lattice constant determined. As seen in figure 2, MoS_2 has a hexagonal crystal structure. The materials investigated in this project all have a hexagonal layered crystal structure.

3.4. Convergence testing

Before running the final model, several parameters need to be determined by a convergence test. This was achieved by plotting the change of the parameter against the total energy of the system after an scf calculation. The optimal value could be obtained through convergence, or in the case for the lattice constant by the global minimum.

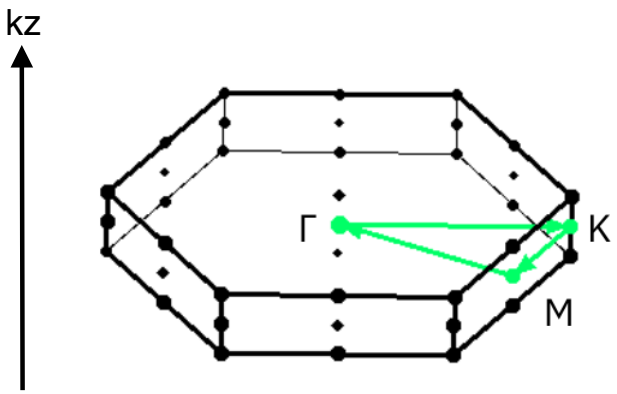

Figure 4: The first Brillouin zone and the high symmetry points of MoS_2 and k wavevector path [Γ,K,M,Γ] where Γ =(0,0,0), K=(0.6667,-0.3333,0) and M=(0.5000, -0.5000, 0). These were chosen with the aid of XCrySDen [25].

The kinetic energy cutoff for wavefunctions (ecutwfc) and as a consequence, the kinetic energy cutoff for charge density and potential (ecutrho) are set according to the pseudopotential (PP) used in the calculations. In an ultrasoft PP, it is required to chose an ecutrho value that is larger than the default value of 4 times the ecutwfc. This is due to the shape of augmentation charge, and testing is required to find suitable values. It was sufficient in the case for MoS_2 to use 5 times the ecutwfc for the ecutrho parameter. Looping through and finding a suitable value for the ecutwfc, next, the number of k points generated was tested. Similarly to the ecutwfc, an ideal value for the k points was obtained through looping a list of values. The lattice parameter was obtained by looping through various values and inspecting the minimum value.
The convergence values for monolayer MoS_2 were determined by convergence testing as seen in figure 4. In a similar process the values for the bilayer material were also identified to be the same. Ideally, high values would be chosen for the ecutwfc and k points. However, given the amount of computational time and expensive that would incur, the values obtained from the convergence tests were used in the final calculations for the band structure and DOS. The ecutwfc is set to 150 R_y, the k point grid to 15 by 15 by 1 and the lattice constant to 6.074 Bohr for MoS_2 monolayer and bilayer. Consistently through out all calculations made in the project, the same ecutwfc and k point grid was used as all convergence testing conveyed this was suitable.

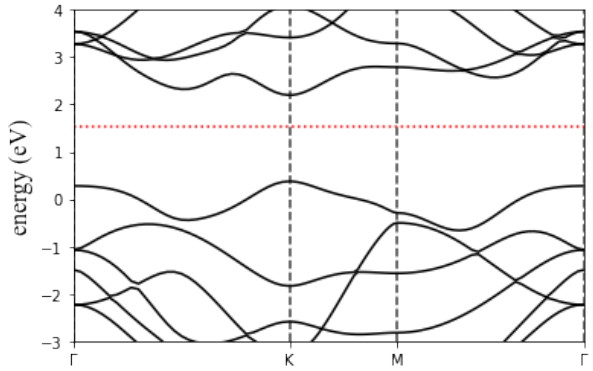

(a) Bands structure diagram of monolayer MoS_2. Fermi energy = 1.520 eV.

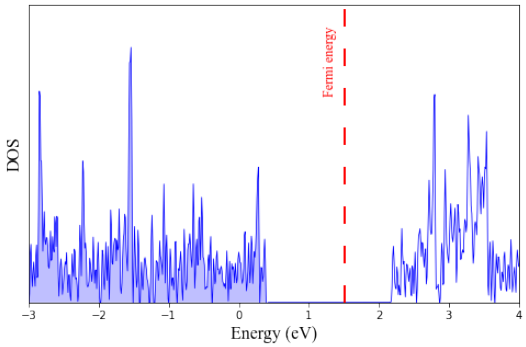

(b) Density of states plot of monolayer MoS_2. Fermi energy = 1.520 eV.

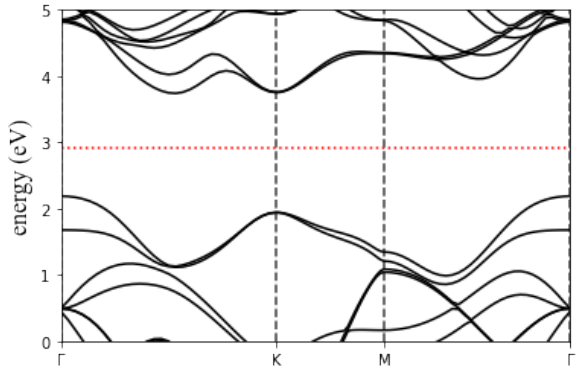

(c) Band structure diagram of bilayer MoS_2. Fermi energy = 2.921 eV.

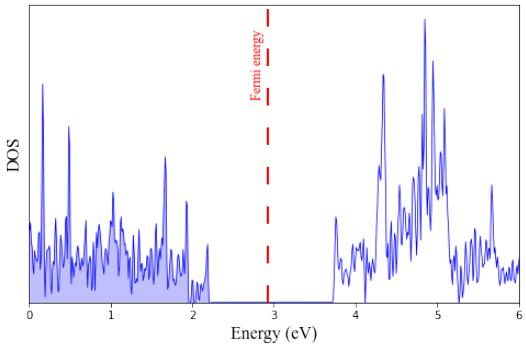

(d) Density of states plot of bilayer MoS_2. Fermi energy = 2.921 eV.

Figure 5: Comparison of the band structure and density of states for MoS_2 monolayer and bilayer, respectively. The red dashed line indicates the Fermi energy. The energy gap calculations can be extracted from the *dos.dat* data output from the QE DOS calculation. (a) at the K wavevector, the highest occupied valence band is aligned with the lowest conduction band and (b) thus, this is a direct semiconductor with energy band gap of 1.810 eV. (c) the highest occupied valence band is at the Γ point whereas the lowest conduction band is at the K wavevector and (d) thus, this is an indirect semicondutor with an energy band gap 1.520 eV.

3.5. Band structure and DOS

Plotting the band structure of a material can give us insight into the electrical properties that the material exhibits [19]. Using XCrySDen, the Brillouin zone (BZ) can be determined from the QE output [25]. Figure 4, it was shown that the reciprocal lattice also forms a simple hexagonal lattice. Notably, in order to achieve a single layer structure (or MoS_2 in this section), the separation in real space is taken to be as large as possible so that there is negligible interaction between nearby repeating structures. Therefore, this will invoke a very thin BZ in the reciprocal z axis, figure 4.

The script that is submitted in this procedure performs a final SCF and NCSF

calculation. Then proceeds to compute the band structure and DOS using the bands.x and dos.x modules. The final SCF calculation calculates the eigenvalues and outputs the final converged values given the convergence tests that were done previously. The NSCF calculation provides an update to the value of the Fermi energy, required when the band structure and DOS are plotted to gain the full picture of what the electronic properties are. The band calculation is also strictly speaking an NSCF calculation too. However, here the eigenvalues are calculated along a specified k-path, which is determined in this project with ease using XCrySDen. Lastly, the DOS is also calculated and plotted to provide an alternative view of the electronic properties of the material. In figure 5 the plots for band structure and density of states for both a monolayer and bilayer of MoS_2 can be observed.

The energy band gap expected for MoS_2 is 1.6 eV and 1.26 eV for monolayer and bilayer MoS_2 [8]. The results that have been presented by these calculations do not agree entirely with the results in the literature found. However, figure 5 does indicate that there is a drop off in the energy band gap value as the structure gets thicker. By the density of states plots, it can be seen that no electrons occupy states in the conduction band. Given the narrow energy band gap between the highest occupied state and the lowest unoccupied state, the results displayed throughout this section confirm that MoS_2 is a semiconducting material. Furthermore, there is validation to the results seen in [8], where the type of semiconductor changes depending on the material being a monolayer or in bulk. Using QE to valid this result gives the results established in the next section confidence, since they adhere to the methodology used here.

4. Results and Discussion

Materials with an odd number of electrons in the unit cell can be expected to be metals due to always having one band that is not completely occupied. The focus on materials with a less straightforward conclusion on the electronic properties have been explored and discussed in this section. In figure 4 all band structure calculations were obtained across the same path along the Brillouin zone at the high symmetry points Γ, K and M.

4.1. Structural and electronic properties of Ta_2C

In figure 6, the relaxed configuration of 2D Ta_2C monolayer from the top and side view are presented. The structure has a lattice constant of 3.056 Å. In 2018, the lattice constant of Ta_2C was found to be 3.08 Å, which is within a 1% tolerance to the value found here [5]. The bond length between the carbon and tantalum atoms throughout the structure was 2.137 Å. The calculated pressure of the structure was -0.46 kbar. For Ta_2C, the Fermi energy is calculated as -0.1709 eV, and is consistent between the SCF and NSCF calculations. Figure 7, as expected the results for Ta_2C determine that the structure is a metal, [5]. The energy band gap was determined by looking at the raw data file *dos.dat*, produced by the DOS calculation using QE. There is a significantly small energy band gap of ≈ 0.30 eV between the valence and conduction bands at the M point, to further conclude that this material is metal.

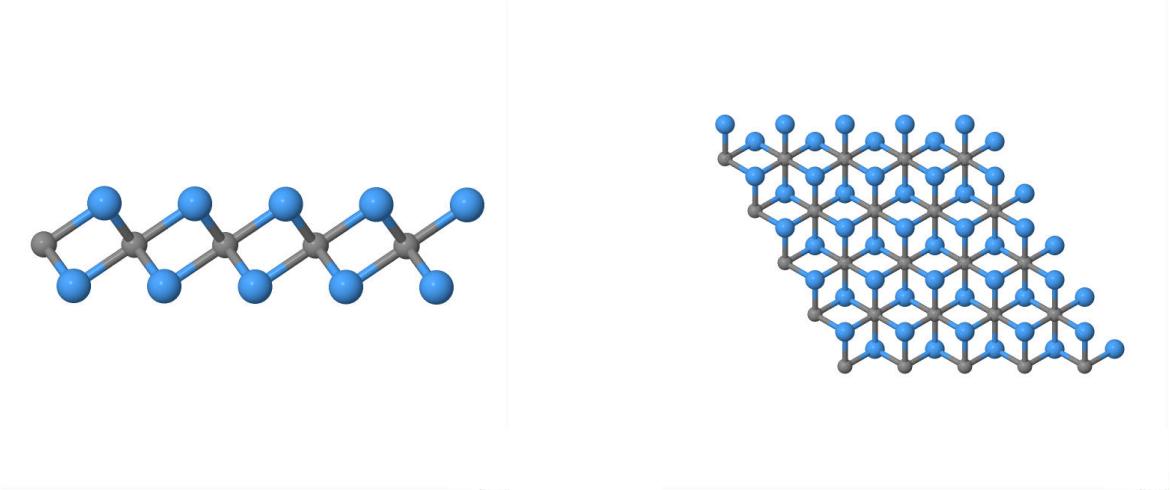

(a) (b)

Figure 6: (a) Side and (b) top view of 2D Ta_2C monolayer. The grey and blue atoms indicate carbon and tantalum respectively. The structure has a lattice constant of 3.056 Å.

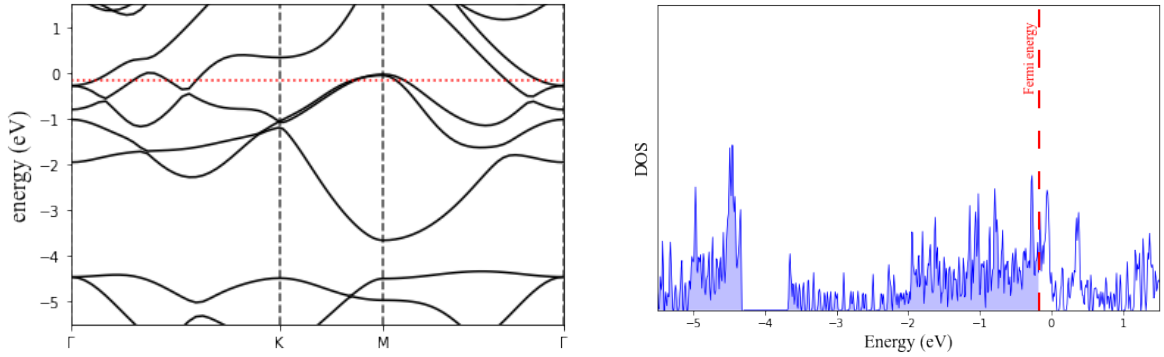

(a) Band structure diagram. (b) Density of states plot.

Figure 7: The electronic properties for Ta_2C monolayer, demonstrated by (a) band structure diagram and (b) density of states plot. The red dashed lines represent the Fermi energy at -0.1709 eV and resides within the conduction bands. Ta_2C is a metal [5].

4.2. Structural and electronic properties of Ta_2CH_2

Before the calculation of Ta_2CH_2, the structure Ta_2CH was first calculated and explored in order to build up the atomic positions of the crystal. Ta_2CH has an odd number of electrons per unit cell, therefore can be confirmed as a metal. With that stable structure obtained by the usual VCR looping protocol, by symmetry, another hydrogen atom was placed on the underside of the MXene layer, figure 8. The lattice constant Ta_2CH_2 is 3.088 Å. The bond length between the Ta and C atoms was 2.172 Å, which has stretched out compared to Ta_2C. This material had a pressure of -0.13 kbar. In figure 9, the bands

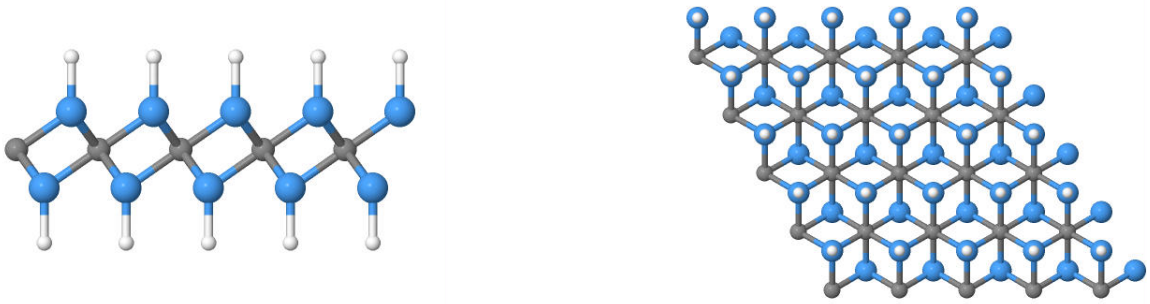

(a) (b)

Figure 8: (a) Side and (b) top view of 2D Ta_2CH_2. The grey and blue atoms indicate carbon and tantalum respectively. White atoms correspond to the Hydrogen surface terminal groups. The lattice constant was 3.088 Å.

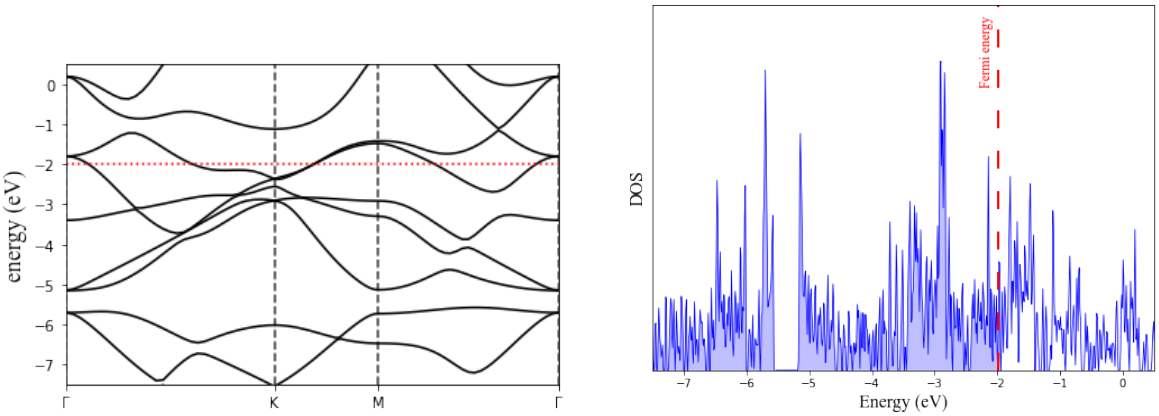

(a) Band structure diagram. (b) Density of states plot.

Figure 9: The electronic properties for Ta_2CH_2 monolayer, demonstrated by (a) band structure diagram and (b) density of states plot. The red dashed lines represent the Fermi energy at -1.977 eV and resides within the conduction bands. Ta_2CH_2 is a metal.

calculation shows that the Fermi level resides within the conduction bands. Thus, as demonstrated by the density of states, some electrons occupy the lower level conduction bands, figure 9b. The smallest energy gap between the valence and conduction bands appears between the Γ-K direction on the Brillouin zone, with an energy gap of 0.36 eV. The results indicate that Ta_2CH_2 is a metal due to the occupation of the electrons in the conduction band below the Fermi level.

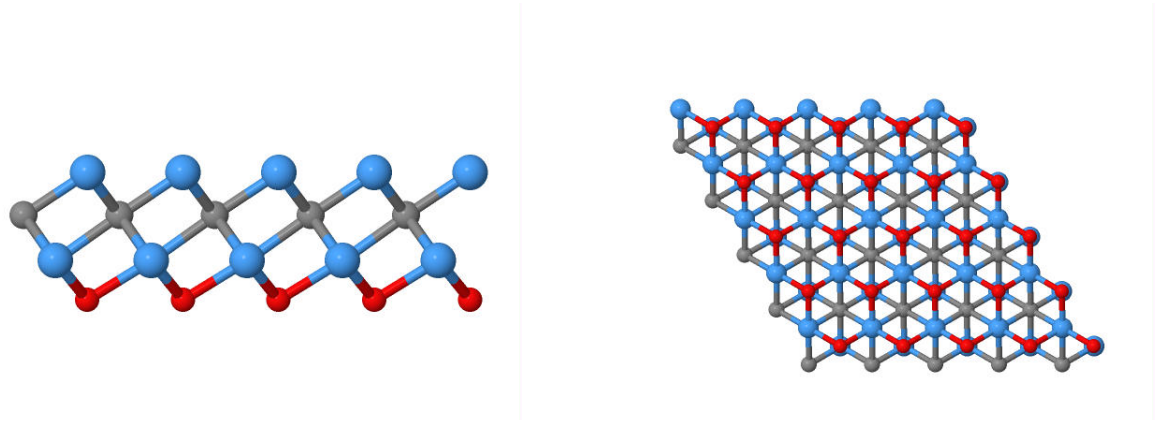

(a) (b)

Figure 10: (a) Side and (b) top view of 2D Ta_2CO monolayer. The grey and blue atoms indicate carbon and tantalum respectively. Red atoms correspond to the oxygen atoms. The lattice constant is 3.076 Å.

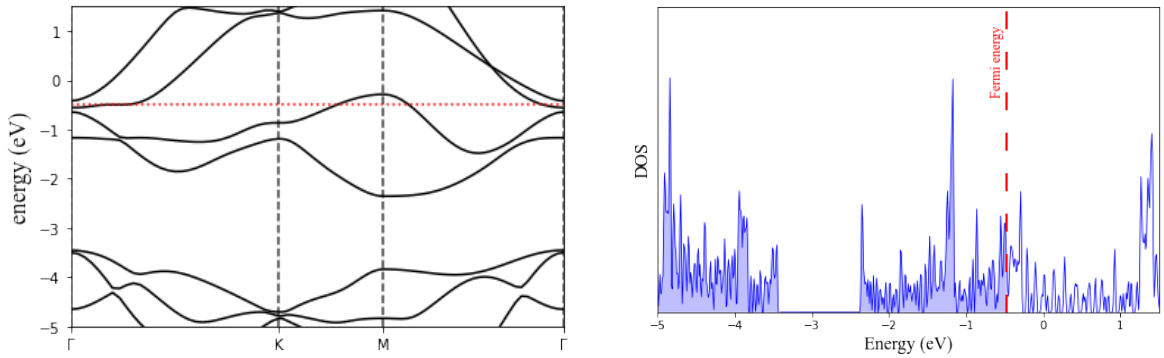

(a) Band structure diagram. (b) Density of states plot.

Figure 11: The electronic properties for Ta_2CO monolayer, demonstrated by (a) band structure diagram and (b) density of states plot. The red dashed lines represent the Fermi energy at -0.478 eV and resides within the conduction bands. Ta_2CO is a metal.

4.3. Structural and electronic properties of Ta_2CO

In figure 10, the relaxed structure of Ta_2CO has a lattice constant of 3.076 Å. The bond length between the Ta and Carbon atom is 2.175 Å. The angle between the bonds of Ta-O-Ta is 95.4°. The structure had a final calculated pressure of 0.15 kbar and the Fermi energy is at -0.4784 eV. The smallest energy band gap that occurs is at the M point with 0.71 eV. The results indicate that Ta_2CO is a metal due to the occupations of the conduction band below the Fermi level.

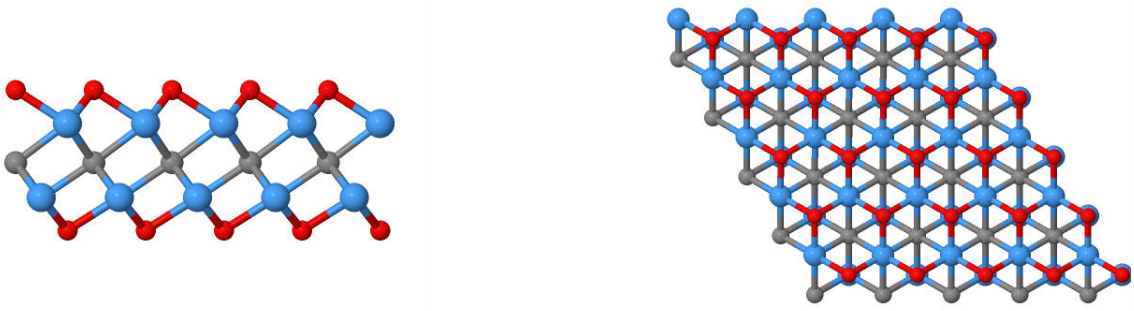

(a) (b)

Figure 12: (a) Side and (b) top view of 2D Ta_2CO_2. The grey and blue atoms indicate carbon and tantalum respectively. Red atoms correspond to the oxygen atoms. The lattice constant was 3.065 Å.

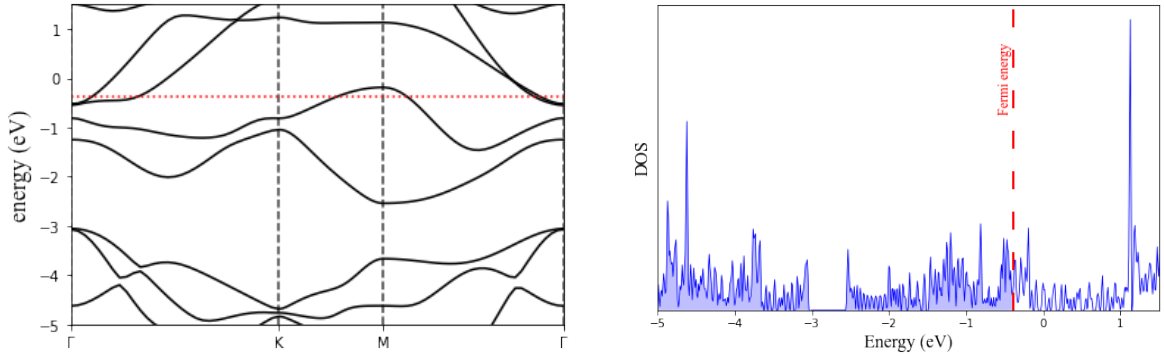

(a) Band structure diagram. (b) Density of states plot.

Figure 13: The electronic properties for Ta_2CO_2, demonstrated by (a) band structure diagram and (b) density of states plot. The red dashed lines represent the Fermi energy at -0.478 eV and resides within the conduction bands. Ta_2CO_2 is a metal.

4.4. Structural and electronic properties of Ta_2CO_2

The final relaxed configuration of Ta_2CO_2 had lattice constant of 3.065 Å, figure 12. The oxygen atom bonded to neighbouring tantalum atoms with an angle of 94.2° between the bonds. The relaxation calculated a pressure of -0.35 kbar. In figure 13, the smallest energy gap between the valence and conduction bands is 0.13 eV. The highest valence bands being at Γ points and the lowest conduction bands appearing at M points. The Fermi level is -0.382 eV. The results indicate that Ta_2CO_2 is a metal due to the occupation of the electrons in the conduction band below the Fermi level.

(a) (b)

Figure 14: (a) Side and (b) top view of 2D Ta_2CS. The grey and blue atoms indicate carbon and tantalum respectively. Yellow atoms correspond to the sulphur atoms. The lattice constant was 3.143 Å.

4.5. Structural and electronic properties of Ta_2CS

The final calculated structure of Ta_2CS has a lattice parameter of 3.143 Å, figure 14. The sulphur atom bonds to the tantalum atoms similarly to the oxygen surface terminal groups. The bond length between the carbon and tantulum atoms is 2.21 Å. The angle made between the bonds of Ta-S-Ta is 80.2°. From the band structure and DOS calculations, it can be determined that the Fermi energy is 0.274 eV. The band gap is located between -6 eV and -5 eV, fig. 15b. The band gap is $\approx$ 0.1 eV, between Γ-K. However, more calculations need to be made in order to get a truer representation of the size of this energy gap and hence its approximation here. It was deduced that Ta_2CS is a metal due to the occupation of the conduction bands below the Fermi level and small energy band gap.

4.6. Structural properties of Ta_3C_2

Conclusions can be made about Ta_3C_2 given that there are an odd number of electrons per unit cell, thus making the material metal. In figure 16, the structure of Ta_3C_2 was calculated with lattice constant was 3.111 Å and the bond length between the Ta and C atoms was 2.236 Å. The relaxed structure had a calculated pressure of -0.41 kbar. This pressure is closer to zero compared with the one that was obtained by the VCR loop for Ta_2C. Ta_3C_2 opens up an opportunity to extend the investigations into surface terminal groups such as H_2, O and O_2 and the electronic properties of these thicker MXene structures.

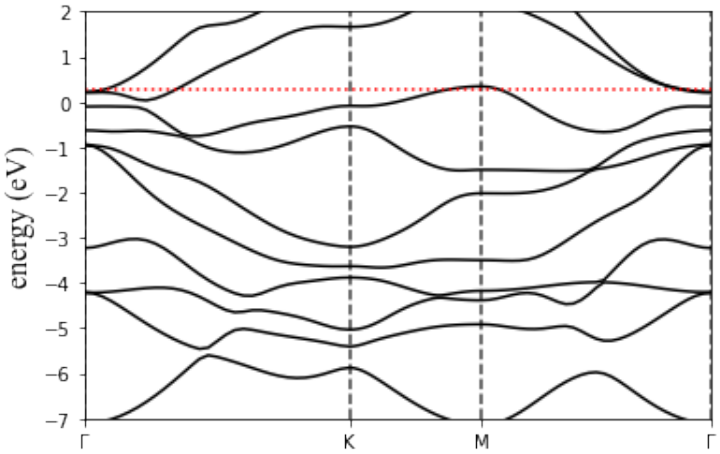

(a) Band structure diagram.

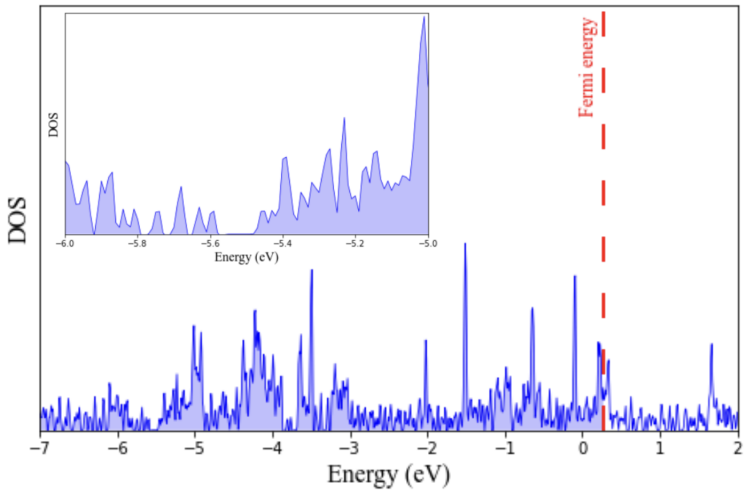

(b) Density of states plot.

Figure 15: The electronic properties for Ta_2CS, demonstrated by (a) band structure diagram and (b) density of states plot. (b) A closer look at the energy gap can be observed in the subplot, where the energy gap between the lowest conduction band and the highest valence band is ≈ 1.0 eV. The red dashed lines represent the Fermi energy at 0.274 eV and resides within the conduction bands. Ta_2CS is a metal.

4.7. Other materials considered

Other materials such as: Ta_2CF_2, $Ta_3C_2H_2$, $Ta_3C_2O_2$ and Ta_4C_3, were also investigated. However, at this current time, it was not possible to obtain convergence in the calculations for these structure. In particular for Ta_2CF_2, the calculations were unable to be repeated despite the results found in the literature [5]. It can be seen in the literature that Ta_2CF_2 has been confirmed as a metal.

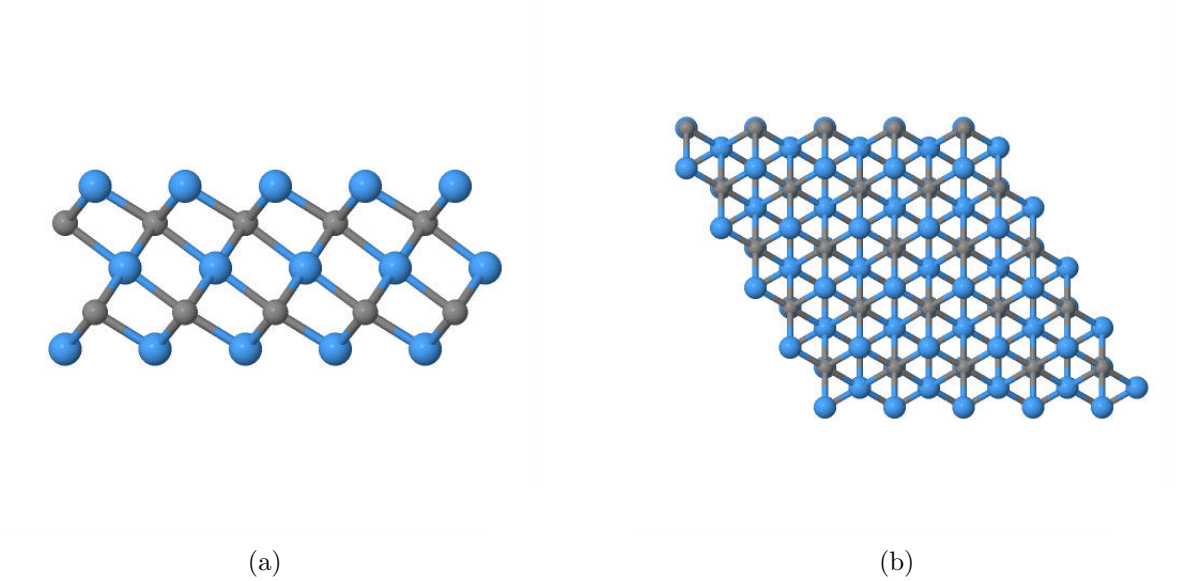

(a) (b)

Figure 16: (a) Side and (b) top view of 2D Ta_3C_2 monolayer. The grey and blue atoms indicate carbon and tantalum respectively. The lattice constant was 3.111 Å.

4.8. Future considerations

Continuing this line of investigation, the next steps would be to expand on the surface terminal groups used and explore the possibility of using DFT to model other MXenes consisting of other transition metals. For example, another tranisition metal of interested could be Tungsten. It would also be possible to replace the carbon atoms in all of the structures reported with nitrogen, and report on the calculations of these materials. It was very challenging to replicate the modelling of Ta_2CF_2 as a material [5]. It may have been possible to have achieved a stable structure through DFT if other pseudopotentials were explored, for example the relativistic pseudopotentials since the atoms that are being modelled are not the lightest. Scalar relativistic pseudopotentials mostly only accound for the relativisitc effects in light atoms. Provided that the Ta_4C_3 MXene has been successfully synthesised by etching, investigating the conductive properties of a thicker MXene with surface terminal groups added would be an interesting next step [26]. As mentioned in the motivation of this paper, another interesting investigation would be to try modelling the electronic properties of MoS_2-on-MXene to explore the possibility of the best material for the electrodes of lithium batteries [27].

5. Conclusion

The implementation of DFT using the package Quantum ESPRESSO was successful at modelling the structural and electronic properties of a material. For example, in the case of MoS_2, it was possible to demonstrate the change to the type of semiconductor the material exhibited by going from a single to a double layer. The introduction of a surface terminal group appeared to always reduce the energy band gap of the materials

electronic structure, i.e bringing the valence band and conduction band energy closer together. It was deduced that the MXene, Ta_2C did not change from being a metal with the addition of the surface terminal groups explored here. In future investigation, there would be potential recalculate these structures with different MXenes. For example, Ta_2N was not investigated during this project. It would also be of interest to expand the types of surface terminal groups explored. The conductive properties of each of these materials could have suitable applications to the design of electrodes on lithium batteries in the future if synthesis through etching, or another technique, is possible.

Acknowledgements

The author would like to highlight appreciation for the collaboration with Lucy Peggs, University of Bath, in order to complete this project. All figures and data outputs in this report were produced by the author. Throughout the project it was most useful to have a partner to aid with troubleshooting and to confer on the underlying theory. This research was supervised by Prof. D. Wolverson, University of Bath, and the support throughout this project was valued. This project made use of the Janus High Performance Computing (HPC) Service at the University of Bath. A special mention to Conn O'Rourke for their assistance as part of the phase-1 users of the newly founded HPC at University. The author is also grateful for his time on placement year with Operational Decision Management (ODM), IBM. The experience gained using virtual machines helped to get XCrySDen working on the Apple Mac 2020 M1 Silicon chip. Lastly, a mention to Dr. Levi Lentz, MIT, who provided online tutorials on how to plot the band structures from the Quantum ESPRESSO outputs via their website: *blog.levilentz.com* . Jmol: an open-source Java viewer for chemical structures in 3D. *http://www.jmol.org/* .

References

[1] Naguib M *et al.* 2012 *ACS Nano* **6**(2) 1322–1331
[2] Kailasa S K *et al.* 2021 *Journal of Molecular Liquids* D **342** 117524
[3] Ming F *et al.* 2020 *Advanced Materials* **33**(1) 2004039
[4] Gouveia J D *et al.* 2021 *Applied Surface Science* **544** 148946
[5] Zhao P *et al.* 2018 *Phys.Chem.Chem.Phys.* **20** 16551
[6] Zhao X *et al.* 2020 *CHEM* **6**(3) 544–546
[7] Tipler P and Llewellyn R (eds) 2002 *Modern Physics* (New York, USA: W. H. Freeman)
[8] Rahman I A and Purqon A 2016 *J. Phys.: Conf. Ser.* **877** 012026
[9] Mostafaei A and Abbasnejad M 2021 *Journal of Alloys and Compounds* **857** 157982
[10] Leach A R (ed) 1996 *Molecular Modelling Principles and Applications* vol 1 (Essex, UK: Addison Wesley Longman Limited)
[11] Guseinov I 1998 *Journal of Molecular Structure: THEOCHEM* **422**(1-3) 69–73
[12] Kohn W and Sham L J 1965 *Phys. Rev.* **140**(4A)
[13] Mostafaei A *et al.* 2019 *Phys. E Low-dimens. Syst. Nanostruct.* **114** 113559
[14] Giannozzi P *et al.* 2009 *Phys:Condens. Matter* **21** 395502
[15] Giannozzi P *et al.* 2017 *Phys:Condens. Matter* **29** 465901
[16] Giannozzi P *et al.* 2020 *Chem. Phys.* **152** 154105
[17] Giustino F (ed) 2014 *Materials Modelling Using Density Functional Theory: Properties and Predictions* vol 1 (Oxford, UK: Oxford University Press)

[18] Honhenberg P and Kohn W 1964 *Phys. Rev.* **136**(3B)
[19] Kittel C (ed) 1987 *Quantum Theory of Solids* vol 1 (Canada: John Wiley & Sons, Inc.)
[20] Smirnov G and Stegailov V 2017 *Journal of Mathematics: LOBACHEVSKII* **38**(5) 974–977
[21] Vanderbilt D 1990 *Phys. Rev. B.* **41**(11) 7892–7895
[22] N Marzari D V *et al.* 1999 *Phys. Rev. Lett..* **82** 3296
[23] Richard J *et al.* 1986 *Phys. Rev. B.* **33** 3778
[24] Meng L *et al.* 2016 *Science and Technology of Advanced Materials* **17**(1) 189–199
[25] Kokalj 2003 *Comp. Mater. Sci.* **28** 155–168
[26] Syamsai R *et al.* 2019 *Journal of Alloys and Compounds* **792** 1230–1238
[27] Chen C *et al.* 2018 *Angewandte Chemie.* **57**(7) 1846–1850